nature photonics

LETTERS

PUBLISHED ONLINE: 10 JANUARY 2010 | DOI: 10.1038/NPHOTON.2009.263

Quantum cascade lasers that emit more light than heat

Yanbo Bai, Steven Slivken, Shigeyuki Kuboya, Shaban R. Darvish and Manijeh Razeghi*

For any semiconductor lasers, the wall plug efficiency, that is, the portion of the injected electrical energy that can be converted into output optical energy, is one of the most important figures of merit. A device with a higher wall plug efficiency has a lower power demand and prolonged device lifetime due to its reduced self-heating. Since its invention, the power performance of the quantum cascade laser[1] has improved tremendously[2–7]. However, although the internal quantum efficiency[7,8] can be engineered to be greater than 80% at low temperatures, the wall plug efficiency of a quantum cascade laser has never been demonstrated above 50% at any temperature. The best wall plug efficiency reported to date is 36% at 120 K (ref. 9). Here, we overcome the limiting factors using a single-well injector design and demonstrate 53% wall plug efficiency at 40 K with an emitting wavelength of 5 μm. In other words, we demonstrate a quantum cascade laser that produces more light than heat.

The core design of a quantum cascade laser (QCL) generally comprises an active region and an injector[1]. In the injectorless design[10,11], however, two adjacent active regions are connected directly. For an injector-based core design, electrons generate photons in the active region through a transition from the upper laser level to the lower laser level. The injector forms a miniband, which blocks electrons from escaping from the upper laser level into the continuum, yet couples strongly to the lower laser level. In addition, this injector, as the name implies, also serves to recycle extracted electrons by re-injecting them into the upper laser level of a subsequent emitting stage. For conventional room-temperature, high-efficiency designs, the implementation of the injector is usually a chirped superlattice, incorporating many pairs of quantum well/barriers. This long injector approach is advantageous for high-temperature operation, because an electron reservoir can be formed at the end of the injector, which helps to reduce thermal backfilling. However, at sufficiently low temperatures, thermal backfilling does not pose a serious problem to device operation due to a smaller thermal activation energy, and the long injector approach starts to present adverse effects[9]. Most obviously, the voltage defect[12], defined as the difference between the energy drop per stage and the emission energy, is very high at low temperatures, which gives rise to a low voltage efficiency[7]. In addition, as the temperature decreases, the slope efficiency saturates at some point and the threshold current stops decreasing. As a result, the wall plug efficiency (WPE) is not always higher at lower temperatures, but peaks at a certain intermediate temperature, for example, 120 K in ref. 9. Attempts have been made to reduce the voltage defect with alternative designs[12,13], but any improvements were achieved at the expense of slope efficiency. To overcome the limiting factors and fully take advantage of a reduced thermal activation energy at low temperatures, we report a single-well injector design specifically made for low–temperature, high-efficiency operation.

The design philosophy is to create a structure with a high internal quantum efficiency and a minimum voltage defect at both the threshold field (turn-on) and at the field that gives negative differential resistance (NDR; turn-off). Figure 1 shows the conduction band and wavefunction diagram of two QCL stages at a design temperature of 80 K. The active region is composed of three quantum wells, featuring a slightly diagonal optical transition and a single phonon resonance relaxation scheme. The optical phonon limited upper laser level (level 4) lifetime, lower laser level (level 3)

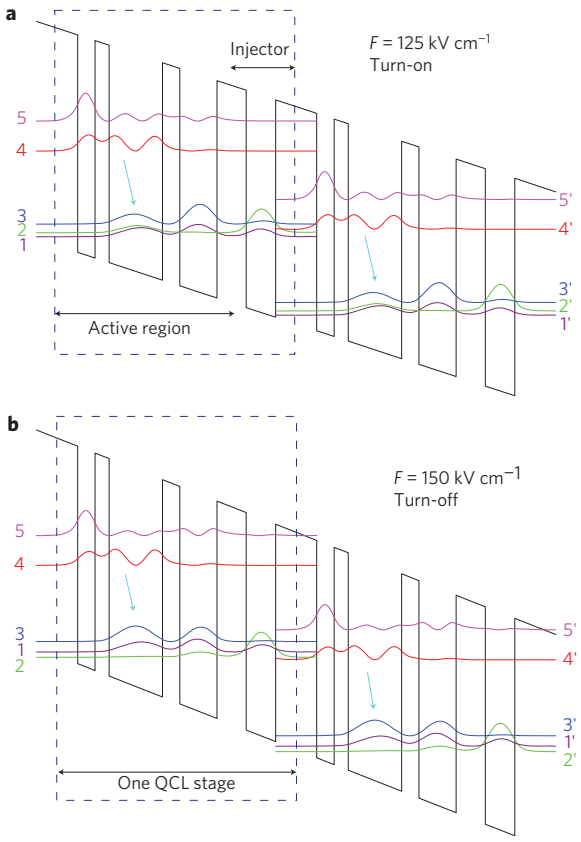

Figure 1 | Conduction band and wavefunction diagram for the single-well injector design. a,**b**, Simulation is performed at turn-on (**a**) and turn-off (**b**) conditions. The dashed box demarcates one full stage. The comb-shaped structure denotes the conduction band diagram of alternating $Ga_{0.34}In_{0.66}As$ (well) and $Al_{0.64}In_{0.36}As$ (barrier) layers. The superimposed horizontal curves are the modulus-squared wavefunctions. The lasing transition takes place from level 4 to level 3, indicated by vertical arrows. Starting with the injection barrier, the thicknesses in nanometres for one QCL stage are (left to right): **3.8**, 1.6, **1.3**, 4.9, **1.6**, 3.4, **2.7**, 2.7, where the AlInAs barriers are in bold, and the underlined thicknesses represent the doped layers (2.2×10^{17} cm^{-3}).

Center for Quantum Devices, Department of Electrical Engineering and Computer Science, Northwestern University, Evanston, Illinois 60208, USA. *e-mail: razeghi@eecs.northwestern.edu

lifetime, and the transition lifetime between level 4 and level 3, are calculated to be 2.17, 0.44 and 6.76 ps, respectively. The internal quantum efficiency is therefore 82%, based on the calculated lifetimes and a simple rate equation approach[8]. The benefit of an active region with a high internal quantum efficiency can be lost if carrier transport is poor[8]. For this reason, we introduced a single quantum well as the injector. Spatially, the injector level (level 2) is located between the active regions of two adjacent stages. Energetically, as the applied field increases, it passes the phonon resonance levels (level 1 and 3), in turn. The structure is carefully designed such that immediately after level 4′ passes level 3, level 2 lies in between level 1 and level 4′ (the scenario in Fig. 1a). At this field, carriers accumulating in level 1 can be thermally activated into level 2 by means of phonon and electron–electron scattering. With the bridging of level 2, level 4′ can be populated via resonant tunnelling through the injection barrier[14]. The unique aspect of this design is the spatial and energetic location of the injector level, which effectively forms a thermal 'forward filling' scheme. This scheme is advantageous for population inversion and carrier transport, which is lacking in injectorless designs[11,12]. The combination of a high internal quantum efficiency and good carrier transport is expected to give a high slope efficiency. In addition, the thermal forward filling scheme allows for a voltage defect of less than one optical phonon energy at the turn-on condition.

As well as a small voltage defect at turn-on, the voltage defect at turn-off should also be minimized, otherwise the device would exhibit a high differential resistance and therefore a lower overall electrical efficiency[7]. The turn-off condition occurs when level 4′ passes the ground level of the injector miniband (Fig. 1b). At this field, level 4′ becomes out of resonance with the injector, and the current decreases as more voltage is applied to the device, that is, NDR behaviour is exhibited. In this design, a three-well active region (single phonon resonance) is used instead of a four-well active region[11] (double phonon resonance), because a minimum energy drop per stage near the NDR field can be achieved with the smallest energy difference between the lower laser level and the ground level of the injector miniband. For this single-well injector design, the turn-off field is only 20% greater than the turn-on field, which is the smallest margin for any existing mid-infrared QCL design. The reduction of the voltage defect at both turn-on and turn-off directly translates into a lower operating voltage per stage, which is strongly favoured for a high WPE. Furthermore, the differential gain is inversely proportional to the period (thickness) of the repeating QCL stage[10]. The period of a typical room-temperature, high-efficiency design at this wavelength is ∼50 nm. The period of this design is only 22.1 nm. As a result, the differential gain is expected to be much higher, which is helpful for a small threshold current density.

The main purpose of this work is to demonstrate the highest WPE possible in pulsed-mode operation. Accurately measuring the output power outside the cryostat window is therefore critical, and requires a regular and stable output far field to maintain a constant optical collection efficiency. We therefore chose to process the QCL wafer into a buried ridge structure (Fig. 2a) with a ridge width only 6 μm wide. The lasing far field was confirmed at room temperature to be regular and stable when driven at currents significantly above threshold (Fig. 2b).

As the differential gain of this structure is designed to be high, a device with a shorter cavity length does not show a large increase in threshold current, yet can show large increases in slope efficiency[7]. Bearing this in mind, we found that the optimum device cavity length is 2 mm for the highest WPE, as opposed to 5 mm for the room-temperature, high-efficiency design[6]. Figure 3 shows the test results for the 2 mm device. At a design temperature of 80 K, the threshold current density, threshold voltage per stage, and slope

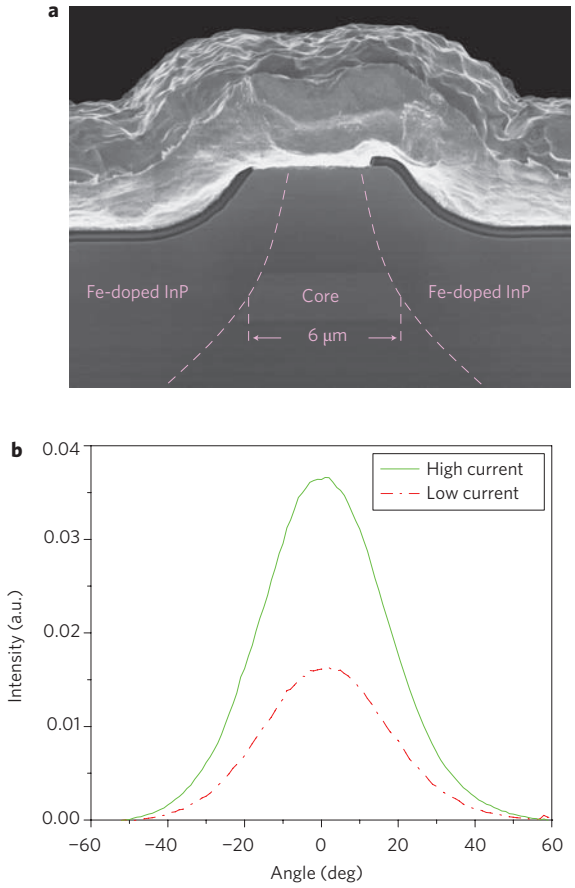

Figure 2 | Image of the device facet and lasing far field. a, Scanning electron microscopy image of a processed device facet showing the buried ridge structure. The lateral regions adjacent to the laser core are filled with iron-doped InP with a resistivity of $\sim 1 \times 10^5\,\Omega$ cm. **b**, Laser angular beam characteristics in the far field taken at 300 K with a 5% duty cycle and 200-ns pulse width. The driving current is $1.2 \times I_{th}$ for the low current and $1.4 \times I_{th}$ for the high current curves, respectively.

efficiency per stage are 0.5 kA cm^{-2}, 0.27 V and 0.17 W A^{-1}, respectively, which are all among the best reported values at a wavelength around 5 μm. The voltage defect at threshold is as low as 22 meV, without subtracting any parasitic voltage drop from the threshold voltage[13]. The temperature-dependent threshold current density, threshold voltage, slope efficiency and maximum WPE are shown in Fig. 3c–f. Above 80 K, due to increased thermal backfilling, the threshold current density increases and the slope efficiency decreases very quickly. Below 80 K, thermal backfilling is mostly negligible. However, similar to ref. 13, the threshold voltage increases as the temperature decreases. This is because most of the carriers are found in the ground level of the injector, so the threshold voltage must be slightly increased to populate the upper laser level. A minimum for the threshold voltage is reached at 150 K, and, at higher temperatures, the behaviour of the threshold voltage is dominated again by thermal backfilling. Consequently, as a collective measure, the WPE peaks at 40 K with a value of $53 \pm 1\%$.

Figure 4 shows the lasing spectra measured slightly above threshold at different temperatures. The behaviour of the temperature-dependent lasing wavelength is the result of two competing effects. On one hand, the conduction band offset decreases with temperature, which always introduces a redshift. On the other hand, the quantum Stark effect can either redshift or blueshift the emission wavelength depending on a decreasing or increasing threshold voltage. Combining these two effects, the experimentally

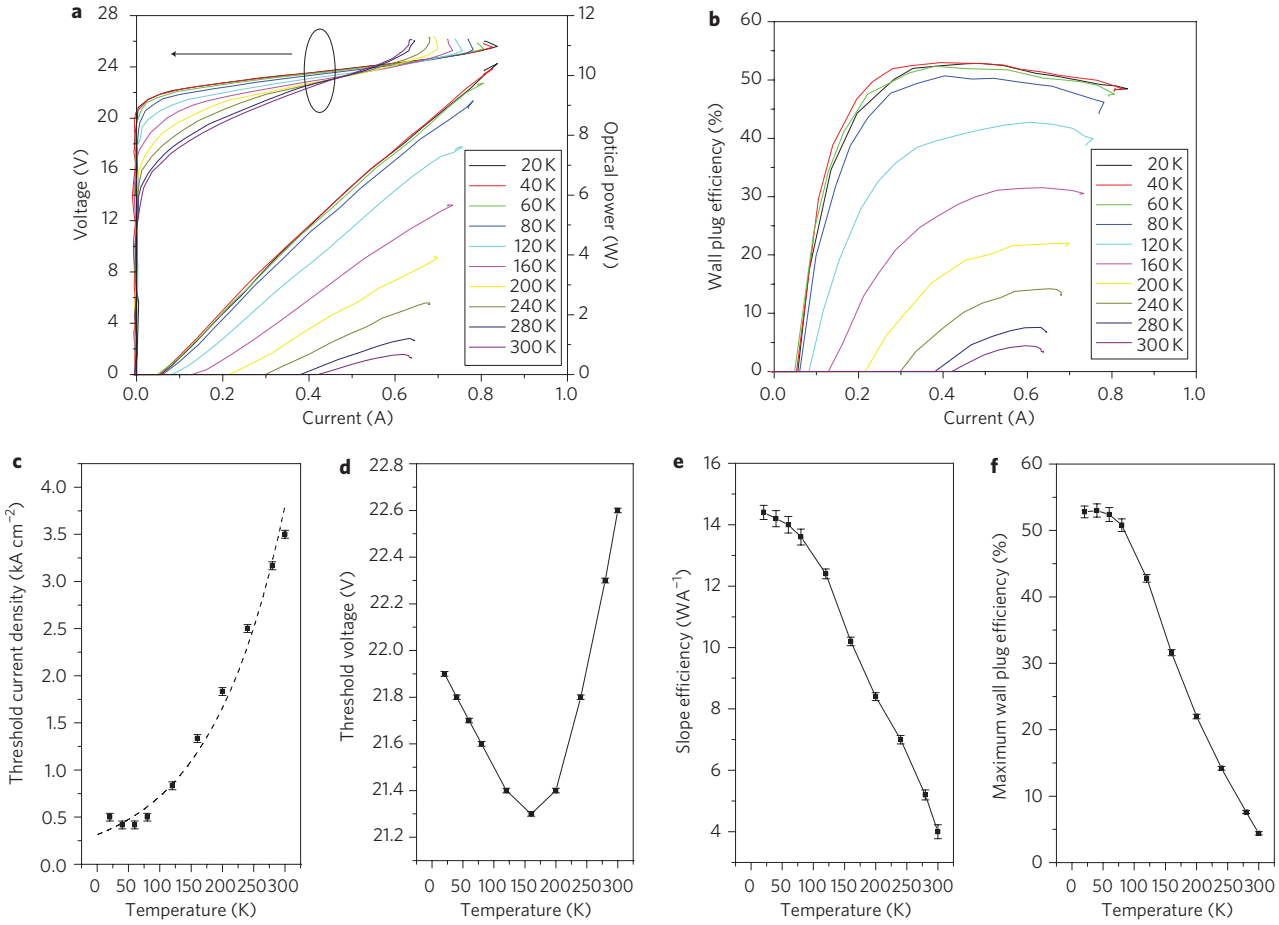

Figure 3 | Temperature-dependent characteristics. a, Power–current and voltage–current characteristics. **b**, WPE–current characteristics. **c–f**, Temperature-dependent threshold current density (**c**), threshold voltage (**d**), slope efficiency (**e**), and WPE (**f**). The dashed curve in **c** is an exponential fit of $J_{th} = J_0 \exp(T/T_0)$, where J_{th} is the threshold current density and T is the temperature. The fitting parameters are $J_0 = 0.3$ kA cm^{-2} and $T_0 = 120$ K. The error bars are generated based on measurement uncertainties for the optical power, current and voltage.

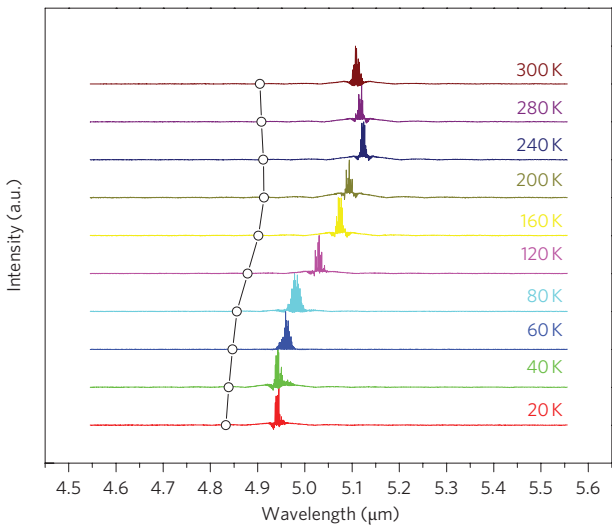

Figure 4 | Lasing spectrum near threshold at different temperatures. The device is biased slightly above threshold in pulsed mode, with 5% duty cycle and a pulse width of 200 ns. The open circles represent the simulated emission wavelength taking into account both temperature-dependent band parameters and the quantum Stark effect.

observed wavelength change as a function of the temperature can be qualitatively reproduced by taking into account the band bowing parameters[15] and the threshold voltage data (Fig. 3d), as shown by the open circles in Fig. 4.

In conclusion, we demonstrate 53% WPE operation of QCLs at 40 K with a single-well injector design. This design takes advantage of a reduced thermal activation energy at cryogenic temperatures to create a thermal forward filling scheme near threshold. This demonstration marks an important milestone in exploring the efficiency capability of intersubband semiconductor lasers.

Methods

Growth and fabrication. The structure was grown in a gas-source molecular beam epitaxy reactor with 80 QCL stages inside the laser core, giving a total core thickness similar to a typical QCL at this wavelength. Growth of the structure started with a n-InP substrate. The layer sequence and the waveguide doping were as follows: 1 μm lower cladding (6×10^{16} cm^{-3}), 80-stage laser core, 3 μm upper cladding (exponentially doped from 6×10^{16} cm^{-3} to 6×10^{17} cm^{-3}) and 1 μm cap layer (2.5×10^{19} cm^{-3}). The QCL wafer was processed into a buried ridge structure. Iron-doped InP regrowth was performed with metal–organic chemical vapour deposition. The fabrication procedure followed the description in ref. 16, except for the use of a AuGe bottom contact to reduce the contact resistance[4].

Device testing. All testing was carried out with a pulse width of 200 ns and a duty cycle of 5% (that is, a repetition rate of 250 kHz). For output power measurement, a calibrated thermopile detector was used to measure the average power, and the peak power was obtained from the measured average power and the known duty cycle. Each device was first tested at 300 K on a thermoelectric cooler by placing the

thermopile directly in front of the laser facet, assuming 100% collection efficiency. Low-temperature testing was carried out with a liquid-helium-cooled cryostat. The same thermopile was placed just outside the cryostat window and the collection efficiency was obtained by comparing the room-temperature power–current curve with that measured outside the cryostat. A collection efficiency of 70% was obtained, which was used to correct the measured power data. In addition, the value was doubled (total peak power) to account for light emitted from the rear laser facet. The noise level of the thermopile was 0.5 mW, which translates to 14 mW for the peak power uncertainty at the relevant duty cycle and collection efficiency. The noise levels of the current and voltage measurements were 5 mA and 10 mV, respectively. Spectra were measured with a Fourier-transform infrared spectrometer (FTIR) with a resolution of 0.125 cm^{-1} in rapid scan mode. Far fields were obtained with a computer-controlled rotational stage and a mercury cadmium telluride (MCT) detector.

Received 10 September 2009; accepted 19 November 2009; published online 10 January 2010

References

1. Faist, J. *et al.* Quantum cascade laser. *Science* **264,** 553–556 (1994).
2. Gmachl, C., Capasso, F., Sivco, D. L. & Cho, A. Y. Recent progress in quantum cascade lasers and applications. *Rep. Prog. Phys.* **64,** 1533–1601 (2001).
3. Evans, A., Yu, J. S., Slivken, S. & Razeghi, M. Continuous-wave operation of $\lambda \approx 4.8$ μm quantum-cascade lasers at room temperature. *Appl. Phys. Lett.* **85,** 2166–2168 (2004).
4. Bai, Y. *et al.* Room temperature continuous wave operation of quantum cascade lasers with watt-level optical power. *Appl. Phys. Lett.* **92,** 101105 (2008).
5. Lyakh, A. *et al.* 1.6 W high wall plug efficiency, continuous-wave room temperature quantum cascade laser emitting at 4.6 μm. *Appl. Phys. Lett.* **92,** 111110 (2008).
6. Bai, Y., Slivken, S., Darvish, S. R. & Razeghi, M. Room temperature continuous wave operation of quantum cascade lasers with 12.5% wall plug efficiency. *Appl. Phys. Lett.* **93,** 021103 (2008).
7. Razeghi, M. High performance InP based mid-IR quantum cascade lasers. *IEEE J. Sel. Top. Quantum Electron.* **15,** 941–951 (2009).
8. Faist, J. Wallplug efficiency of quantum cascade lasers: critical parameters and fundamental limits. *Appl. Phys. Lett.* **90,** 253512 (2007).
9. Razeghi, M. *et al.* High power quantum cascade lasers. *New J. Phys.* **11,** 125017 (2009).
10. Wanke, M. C. *et al.* Injectorless quantum-cascade lasers. *Appl. Phys. Lett.* **78,** 3950–3952 (2001).
11. Katz, S., Vizbaras, A., Boehm, G. & Amann, M. C. High-performance injectorless quantum cascade lasers emitting below 6 μm. *Appl. Phys. Lett.* **94,** 151106 (2009).
12. Dey, D., Wu, W., Memis, O. G. & Mohseni, H. Injectorless quantum cascade laser with low voltage defect and improved thermal performance grown by metal–organic chemical–vapor deposition. *Appl. Phys. Lett.* **94,** 081109 (2009).
13. Escarra, M. D. *et al.* Quantum cascade lasers with voltage defect of less than one longitudinal optical phonon energy. *Appl. Phys. Lett.* **94,** 251114 (2009).
14. Sirtori, C. *et al.* Resonant tunneling in quantum cascade lasers. *IEEE J. Quantum Electron.* **34,** 1722–1729 (1998).
15. Vurgaftman, I., Meyer, J. R. & Ram-Mohan, L. R. Band parameters for III–V compound semiconductors and their alloys. *J. Appl. Phys.* **89,** 5815–5875 (2001).
16. Evans, A. *et al.* Buried heterostructure quantum cascade lasers with high continuous-wave wall plug efficiency. *Appl. Phys. Lett.* **91,** 071101 (2007).

Acknowledgements

The authors would like to acknowledge the support, interest and encouragement of R. Leheny, H. Temkin and M. Rosker from the Defense Advanced Research Projects Agency, M. E. Gross from the Office of Naval Research, and experts from the Naval Research Laboratory and the Army Research Office.

Author contributions

Y.B. designed the laser core structure, fabricated the device, performed the testing and wrote the paper. S.S. designed the waveguide structure, grew the wafer with GS-MBE and wrote the paper. S.K. carried out buried ridge regrowth with MOCVD and S.R.D. conducted the regrowth processing. M.R. provided the idea and supervised the project.

Additional information

The authors declare no competing financial interests. Reprints and permission information is available online at http://npg.nature.com/reprintsandpermissions/. Correspondence and requests for materials should be addressed to M.R.